Journal of Ambient Intelligence and Humanized Computing (2023) 14:13683–13696
https://doi.org/10.1007/s12652-022-04023-4

ORIGINAL RESEARCH

Effective feature extraction for Cerebral Microbleed detection using Edge Emphasized Weber Maximum Directional Co-occurance Matrix

Berakhah F Stanley[1] · **S. Wilfred Franklin**[2]

Received: 30 January 2021 / Accepted: 30 May 2022 / Published online: 25 June 2022

Abstract
CMBs are the accumulations in the brain vessels of many aged and stroke-affected persons. The presence of CMBs may lead to dementia, traumatic brain injury, and other physiological complications leading them to confusing behavior. Tracking of CMBs from the human brain is challenging due to their small size, manual detection by neurologists may lead to delusions. In this paper, we propose a newfangled technique for feature extraction in the detection of CMB, namely the Edge Emphasized Weber Maximum Directional Co-occurance Matrix (EEWMDCM). Our proposed methodology efficiently recognizes the CMB from magnetic resonance images by integrating the WLD with the notions of the Directional Co-occurance Matrix. When compared with the previous works that occupied many handpicked ROIs selections, more useful features can be extracted in our proposed work from the segmented images that progress the accuracy rate in the detection process. Noise removal filters are utilized and the segmentation is done to identify the candidate in the preprocessing stage which strengthens the feature extraction stage. The features that are extracted from the feature extraction stage are classified and experimented with a set of classifiers, the Support Vector Machine (SVM), Cosine Distance (CO) classifier, Chi-square (CS) classifier, Extreme Learning Machine (ELM), and Convolutional Neural Network (CNN) classifier. The proposed work has been verified and validated on an SWI-CMB dataset that was captured from 320 subjects, in which the images from 230 subjects are for training and images from 90 subjects are for testing purposes. The experiential results specify that our proposed work gives the best sensitivity of 97.11%, the precision of 97.31%, specificity of 97.24%, and an accuracy of 98.06%.

Keywords CMBs · Susceptibility Weighted Imaging · Co-occurance Matrices · Kirsch compass method · Weber Local Descriptors · MRI

1 Introduction

A mini-abnormal structure in the brain vessels that are generated by the deposits of blood products is known as CMBs. These types of mini-structures are very common in persons who are affected by Alzheimer's disease, stroke, and TBI (Greenberg et al. 2009; Yates et al. (2014). The human brain normally has the forebrain, the midbrain, and the hindbrain in which, the major portion of the human brain is the cerebrum, which is an element of the forebrain that controls all the muscular activities. Sangiem et al. (2019) noted that the forebrain controls speaking, seeing, smelling, and testing capabilities too. The presence of CMBs will affect the forebrain thus leading to a confusing behavior for the day-to-day activities. According to recent research, CMBs may have a true influence on cerebral function and progress to recognizable destruction such as dementia as explained by Charidimou et al. (2013) and Martinez-Ramirez et al. (2014). CMBs in the brain are correlated with advancing age, and a spike in CMBs is associated with advancing age, and also the presence of CMB may multiple within an image. The risk of this disease depends on the number of CMBs present in the brain. These CMBs are 2–10 mm in size. The most significant risk factor for CMB is hypertension. The existence of CMBs leads to various diseases such as cerebral amyloid angiopathy and cerebral vessel diseases. Sometimes, these structures can also be seen even in healthier persons. If unnoticed, it also damages the surrounding parts of brain tissues.

The manual identification of CMBs by radiologists is difficult due to their small size. The manual detection of CMBs makes identification risky because it has many challenges. Some of them are the time for detection, prompt

✉ Berakhah F Stanley
berakhahfstanley@gmail.com

[1] Arunachala College of Engineering for Women, Nagercoil, Tamil Nadu, India

[2] C.S.I Institute of Technology, Kanyakumari, Tamil Nadu, India

to errors, limited duplicability, and false analysis since the size of CMB is much small. Therefore, automatic detection is needed for the correct diagnosis for the physicians. The most effective diagnostic methodologies for CMBs identification are computed tomography (CT) and magnetic resonance imaging (MR). Due to the ionizing radiation effect of CT scanners, MR imaging, specifically with contemporary improvements such as gradient-echo (GRE-T1 and T2) and susceptibility-weighted imaging (SWI), is frequently favored in clinical practice over CT imaging. After 7–10 days, the CT density of the lesions in CMBs rapidly declines, and they become isodense lesions to the brain. CMBs tend to be detectable on MR images for a long time. Therefore, the CMBs can be captured by SWI, T1 weighted Imaging, and T2 weighted Imaging systems in MRI Imaging (Stanley et al. 2022). The CMBs are more visible in SWI Imaging systems and so the radiologists prefer the Susceptibility Weighted Imaging (SWI) type of MRI for the perfect identification of CMBs.

Some CMB mimics appear in MRI imaging, causing the radiologist to mistakenly label these mimics as CMB. Figure 1 shows a detailed comparison of CMB and CMB mimics. Extracting features from the input image for classification is a crucial task in the detection of CMB. The effectiveness of the feature extraction method creates a great impact on the output accuracy of the detection schemes. Hence, developing an efficacious feature extraction is the main goal of the proposed approach. The developed model should have less complexity to reach the objective of the detection scenario. The main disadvantage of the deep learning approaches is the unavailability of training data. In our proposed method, this limitation is overcome by our proposed method by attaining better accuracy and sensitivity results with limited training data. Also, the utilization of the optimal features for classification yields promising results and this shows the effectiveness of the proposed work.

Abbreviations	
CMB	Cerebral Microbleed
EEWMDCM	Edge Emphasized Weber Maximum Directional Co-occurance Matrix
WLD	Weber Local Descriptors
SVM	Support Vector Machine
CO	Cosine Distance
CS	Chi-square
ELM	Extreme Learning Machine
ML	Machine Learning
CNN	Convolutional Neural Network
FCCA	The fuzzy c-means clustering algorithm
MRI	Magnetic Resonance Imaging
TBI	Traumatic Brain Injury
YOLO	You Look Once
BET	Brain Extraction Tool
ANT	Advanced Normalization Tool
COM	Co-occurance Matrix
DE	Differential Excitation component
GO	Gradient Orientation component
CT	Computed Tomography

2 Related works

Many automated methods have been proposed by many researchers; Dou et al. (2016) suggest that some of the researchers selected the features based on the information about intensity, shape, and size. The radon transform is used in Fazlollahi et al. (2014) to identify the shape information of CMB. Radial Symmetry Transform (RST) is used to describe the spherical regions in Kuijf et al. (2012). 2D fast RST is proposed by Bian et al. (2013) to extract geometric features. Barnes et al. (2011) used a Support Vector Machine (SVM) classifier to classify the

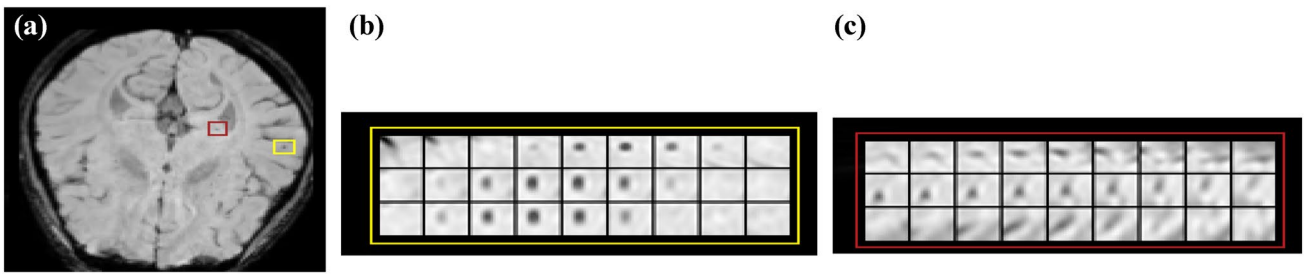

Fig. 1 Pictorial representation of CMB and CMB mimics. The yellow portion represents the presence of CMB and the other red portion is the CMB mimic

CMB images from the features that are obtained with the help of shape and intensity. Van Den Heuvel et al. (2015) have commented that to improve the speed of detection, some researchers removed the CMB mimics first and then the CMB areas are chosen for further processing. A multi-modal method based on enhancing the intensities was implemented in Marcel et al. (2009). This improves the image contrast and eliminates the de trop tissues.

For detecting the CMBs, Mohammed et al. (2018) proposed a technique that utilizes Gray-Level Co-Occurrence Matrix (GLCM), Local Binary Pattern (LBP), and Histogram of Oriented Gradient (HOG) for feature extraction. The feature vectors from each of the techniques are then classified with the help of the k-Nearest Neighbor (k-NN) classifier. Seghier et al. (2011) has proposed a deterministic segmentation method for detecting the CMBs, in which the input images are from T2-Weighted MRI scan images. This method detects the CMBs in 8 patients from a total of 13 more successfully but missed its ability when the subjects had only one CMB. Now, deep learning and the convolutional neural network gets attracted to the detection of medical images. In such a way, in most of the recent works, a two-layered network was proposed, in which the first layer is fully based on the candidate proclamation and classification stage for the reduction of false positives that were proposed in Dou et al. (2016), Liu et al. (2019), Chen et al. (2019), Abro et al. (2020), Ullah et al. (2021), Stanley et al. (2022) Wang et al (2019) and Hong et al. (2019). Hong et al. (2019) proposed a 2D ResNet architecture for retrieving the 2D CMBs from 3D and achieved a sensitivity of 95.71% and an accuracy of 97.46%. But, the execution time and the computational complexity are more. Dou et al. (2015) proposed a technique based on the value of threshold T and used a convolutional Independent Subspace Analysis (ISA) network for the extraction of 3D features, which is followed by a classification phase that eliminates all false positives. This approach achieves 89.44% performance with a false positive rate of 7.7.

A two-stage approach was introduced for the detection of CMB in Dou et al. (2016) and this method uses 3D FCN for the candidate detection and 3D CNN for discriminating the CMBs. This method gives a precision of 44.31% and an average number of false positives per subject of 2.74. The CNN can also be used in various signal process applications such as earthquake detection as proposed in Abdalzaher et al. (2021a, b), etc. Abdalzaher et al. (2021a, b) has compared and evaluated the performance of the proposed work with various ML classifiers. Many of the ML classifiers increase the performance and efficiency of the proposed work as proposed in Moustafa et al. (2021). A two-stage technique with the integration of YOLO and CNN was recently presented in Al-masni et al. (2020) for the automated recognition of CMBs, this framework gives a precision of 61.9%, a sensitivity of 88.3%, and an average false positive rate of 1.4. Many types of linear and non-linear classification models are available. Some of the linear models discussed in Moustafa et al. (2021) are logistic regression, SVM, ridge, Gaussian Naïve Bayes, linear and discriminant analysis and the non-linear models are adaboost, catboost, k-nearest neighbor classifiers.

Because of the small size of CMB and by the confusion raised between CMB and CMB mimic, accurate results of CMB detection were not attained by the state-of-the-art techniques which were discussed above. Also, the methods using CNN consume more time and are more complex. The extraction of optimal features for classification is a challenging task in CMB detection. In our proposed method, the utilization of a weber local descriptor influence the enhancement of edges in the input images, and more accurate features are extracted for classification. Further, the calculation of maximum directional features using energy functions and estimating the co-occurance matrix features from the maximum directional images yields more prominent features which in turn produce better results in classification. The statistical and hierarchical features obtained from the co-occurance matrix produce good results in the detection of CMBs and non-CMBs. The main aim of this paper is to increase the accuracy rate and sensitivity rate in the detection of CMBs. The main contributions are as follows.

1. The feature extraction of the MRI CMB image is done using the proposed Edge Emphasized Weber Maximum Directional Co-occurrence Matrix (EEWMDC) method. Weber Local Descriptors (WLD) principle gives a better performance in identifying the CMBs even when there are any non-monotonous changes in the segmented region. This extracts two components namely the differential excitation and the gradient orientation.
2. Edges are enhanced for the two components of WLD using mean local energy function. From the differential excitation and gradient orientation images, two-directional images are estimated from each of the images using Kirsch edge operator ie, direction (0°(E)), 45°(NE), 90°(N), 135°(NW)) for first image and direction (180°(W), 225°(SW), 270°(S), 315°(SE)) for the second image.
3. Co-occurance matrices are derived from all the directional differential excitation and directional gradient orientation image. The Co-occurrence matrices having the maximum energy values are selected and features are obtained from the selected co-occurrence matrices.

This paper is arranged as follows: The proposed method is well described in Sect. 3. The results and discussions are explained in Sect. 4. Finally, the work is concluded in Sect. 5 with its ideas for future enhancement.

3 Proposed method

Our proposed framework consists of the following stages which are illustrated in Fig. 2. The preprocessing stage uses filters for noise removal and ROI is chosen which is explained elaborately in Sect. 3.1. Section 3.2 reveals the feature extraction stage and Sect. 3.3 describes the classification stage.

3.1 Preprocessing stage

Image pre-processing is the mandatory step in MRI imaging applications. The variations in intensities and the other parameters can be reduced by the pre-processing step. For this, we first, apply the N4 algorithm from the ANTs (Tustison et al. 2010) to correct the input MRI Image. Due to the correction in the MRI input image, the bias field signal will be removed. The non-homogeneities present in the MRI Images and the signals that corrupt the MR Images are known as the bias field signal. This correction also includes the flat-field correction, which assumes only the parametric model.

After these corrections, the input MRI Image is subjected to the BET (Smith et al. 2002). This method is a fast, powerful, and automated tool to separate the brain region alone from the non-brain region. By these automated BETs, the structures over the skull region will be removed. Finally, the image is enhanced to sharpen the regions which are of less intensity due to the formerly applied correction algorithms. Now, the preprocessed image is segmented by FCCA. FCCA is an effective algorithm for image segmentation in various applications such as medical imaging, image analysis, bioinformatics, etc. In this algorithm, at first, the number of clusters is decided, after which a threshold value was set. Based on this threshold value along with the center pixel values, the segmented images are labeled as x or y. Thus, it effectively segments the input corrected MRI Image into two clusters labeled as x for segmented regions with lesions, y for the rest of the area of the brain image without lesions.

Now, to select the segmented region, a thresholding mechanism is used. Since the area of CMB is very small, various parameters based on the size, eccentricity, and roundness are considered for the calculation of threshold value. If the segmented region does not meet the above parameters, then the region is eliminated preserving the regions that meet the above parameters.

3.2 Feature extraction stage

The preprocessed cropped image which is the output of the previous stage is then subjected to the feature extraction stage. Feature extraction is the process of extracting prominent features which will be subjected to classification. A novel method is proposed in this article which is the EEWMDC for the extraction of the features. The powerful texture representation ability of WLD, the detection and enhancing edges using the kirsch edge operator, and the estimation of eminent features from co-occurrence matrices make the feature extraction process more prominent for classification. A brief explanation of the feature extraction methods is described as follows.

3.2.1 Weber Local Descriptors (WLD)

WLD (Chen et al. 2010) is derived from its basic weber's law, which states that a ratio of small increments in the intensity to the intensity of its background is a constant. This can be expressed as follows:

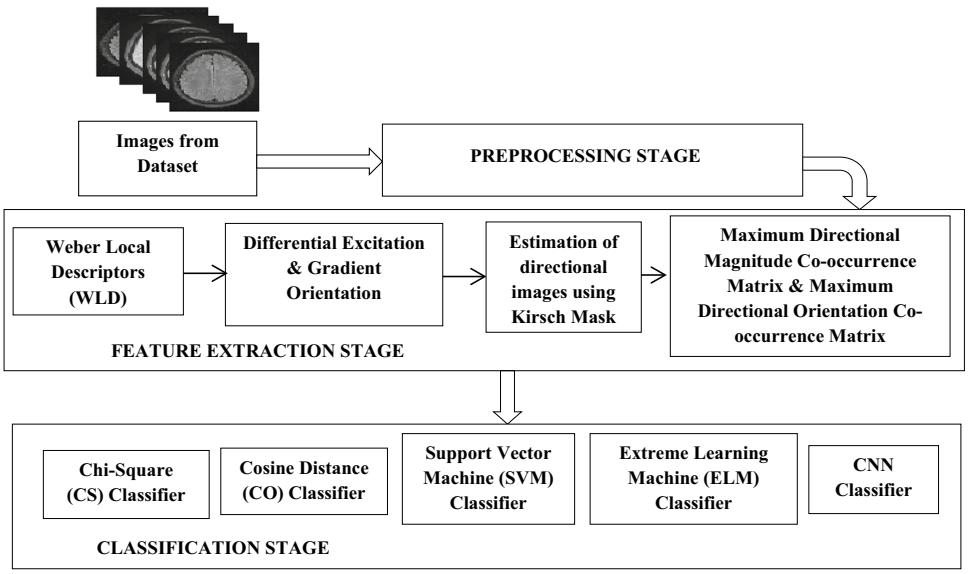

Fig. 2 Overall Block diagram of the proposed method

Fig. 3 Mask filters of Kirsch Compass method

$$d_0: E = \begin{bmatrix} -3 & -3 & 5 \\ -3 & 0 & 5 \\ -3 & -3 & 5 \end{bmatrix} \quad d_1: NE = \begin{bmatrix} -3 & 5 & 5 \\ -3 & 0 & 5 \\ -3 & -3 & -3 \end{bmatrix} \quad d_2: N = \begin{bmatrix} 5 & 5 & 5 \\ -3 & 0 & -3 \\ -3 & -3 & -3 \end{bmatrix} \quad d_3: NW = \begin{bmatrix} 5 & 5 & -3 \\ 5 & 0 & -3 \\ -3 & -3 & -3 \end{bmatrix}$$

$$d_4: W = \begin{bmatrix} 5 & -3 & -3 \\ 5 & 0 & -3 \\ 5 & -3 & -3 \end{bmatrix} \quad d_5: SW = \begin{bmatrix} -3 & -3 & -3 \\ 5 & 0 & -3 \\ 5 & 5 & -3 \end{bmatrix} \quad d_6: S = \begin{bmatrix} -3 & -3 & -3 \\ -3 & 0 & -3 \\ 5 & 5 & 5 \end{bmatrix} \quad d_7: SE = \begin{bmatrix} -3 & -3 & 5 \\ -3 & 0 & 5 \\ -3 & 5 & 5 \end{bmatrix}$$

$$\frac{\Delta x}{x} = K \tag{1}$$

where Δx is the smallest change in intensity when compared to its background. x is the background intensity and K represents constant. The weber local descriptors extract two sets of components. They are differential excitation and gradient orientation.

Differential excitation represents the ratio of the intensity variation between the center pixel and its neighbors to the original image. The arctangent function is applied to this ratio. By this, we get the differential excitation. It is expressed as follows:

$$£(x) = \arctan\left(\sum_n \frac{x_n - x}{x}\right) \tag{2}$$

where x_n is the neighboring pixels and x represents the center pixel. The feature is most probably zero in flat areas and increases when there are discontinuities. But, the small difference in the intensities can have a different problem and it depends on where it occurs in the image. These can be distinguished in a high-intensity region. This is proposed by weber's law very clearly and this can be normalized with the intensity of the pixel itself. The range of £(x) is set in a finite range as $\left(\frac{-\pi}{2}, \frac{\pi}{2}\right)$.

Notations	
Δx	The smallest change in intensity when compared to its background
x	Background intensity
K	Constant
x_n	Neighboring pixels
x	Center pixel
£(x)	Differential excitation
φ(x)	Gradient orientation
g_c	Center pixel
g_i	Neighborhood pixel
N	Total number of neighboring pixels
(DM_i)	Directional Images, where i = 0,1,2,…,7

The gradient orientation can be stated as the ratio of change in intensity in the horizontal direction to the change in intensity in the vertical direction. This extraction is similar to the extraction of components with the help of Sobel operators. This can be expressed as follows:

$$\varphi(x) = \arctan\left(\frac{\Delta H}{\Delta V}\right) \tag{3}$$

where ΔH and ΔV are obtained by the Sobel operator filters.

The precision of the image is magnified by the edge enhancement process using the mean local energy function. This identifies the sharp edge boundaries in an image, such as the edge between a true or false CMB and the corresponding background of an aberrant color, and increases the image contrast in the area shortly around that edge. The advantage is that some imperfections in the image duplication, grains, or noises, or imperfections in the CMBs were not made apparent by this enhancement process. The differential excitation and the gradient orientation components have proceeded with the edge enhancement step through the following expression

$$g_c = \frac{1}{N}\sum_{i=1}^{N} g_i \tag{4}$$

where g_c represents the center pixel, g_i represents the neighborhood pixel and N is the total number of neighboring pixels.

3.2.2 Kirsch compass kernel

Kirsch compass kernel method was introduced by Kirsch (1971) that consists of a single mask which was rotated in eight compass directions such as East (E), North East (NE), North (N), North West (NW), West (W), South West (SW), South (S), and South East (SE) and is represented in Fig. 3. By using the Kirsch compass method, the noises are suppressed and the edge points are preserved.

Each of the mask filters is convolved with the Differential excitation component and Gradient Orientation component, thus producing 8 Directional Images (DM_i), where i = 0,1,2,…,7. From the 8 Directional Images of Differential excitation

Fig. 4 Reckoning the value of the Directional Co-occurance Matrices with the parameters $\theta = 0°$ with distance d = 1 for an image

1	4	3	3	3	2	4
2	1	5	2	1	4	4
3	1	4	4	4	2	5
5	1	3	2	1	4	1
3	3	2	2	1	5	2
4	2	3	3	2	1	1
1	1	3	2	3	4	1

Pixel Values	1	2	3	4	5
1	**2**	0	2	4	2
2	5	1	2	1	1
3	3	3	4	1	0
4	2	2	1	3	0
5	1	2	0	0	0

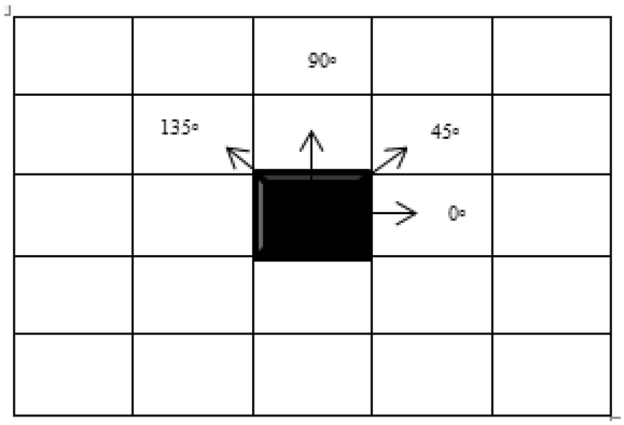

Fig. 5 Determination of Directional Co-occurance Matrices with distance d = 1 in 4 directions (angles)

component, 2 maximum Directional Images are estimated by choosing the maximum pixel values [(DM_i) where i = 0,1,2,3], and [(DM_i) where i = 4,5,6,7]. Similarly, from the 8 Directional Images of Gradient Orientation component, 2 maximum Directional Images are estimated by choosing the maximum pixel values [(DM_j) where j = 0,1,2,3], and [(DM_j) where j = 4,5,6,7].

3.2.3 Extraction of Maximum Directional Co-occurance Matrices

Co-occurance Matrix (COM) is calculated for the maximum directional images obtained from the differential excitation component. Distances with different combinations and directions are demonstrated in Figs. 4, 5, 6 and 7. In this work, two distances (d = 1 and d = 2) with four directions (0°, 45°, 90°, 135°) are used for the COM calculation. Hence 16 co-occurrence matrices are obtained from the Differential Excitation component. Similarly, using the same procedure 16 co-occurrence matrices are obtained from the Gradient Orientation component. The energy values of all the 32 Co-occurance matrices are obtained individually using the following expression.

$$\text{Energy} = \sum_i \sum_j P_{ij}^2 \tag{5}$$

where P_{ij} is the Co-occurance Matrix.

To reduce the redundancy of extracted features, and to increase the effectiveness of detection, the co-occurance matrices with maximum energy values are considered for the extraction of features. Based on the experimental results, 4 Co-occurance matrices are selected with distance, d = 1, and 4 Co-occurance matrices are selected with distance, d = 2. The statistical and hierarchical parameters are estimated from the selected Co-occurance Matrices.

The statistical parameters that are calculated in the proposed work are contrast, correlation, homogeneity, variance, entropy, Sum Entropy, Difference Entropy, shade, prominence, inertia (Haralick et al. 1973; Conners et al. 1984). Thus, we obtain 88 features from the Maximum Directional Magnitude Co-occurrence Matrix and Maximum Directional Orientation Co-occurrence Matrix.

The feature energy (Angular Second Moment) is also known as uniformity or the angular second-order moment and it represents the sum of the square of all the elements in the matrix.

Fig. 6 Reckoning the value of the Directional Co-occurance Matrices with the parameters $\theta = 0°$ with distance d = 2 for an image

1	4	3	3	3	2	4
2	1	5	2	1	4	4
3	1	4	4	4	2	5
5	1	3	2	1	4	1
3	3	2	2	1	5	2
4	2	3	3	2	1	1
1	1	3	2	3	4	1

Pixel Values	1	2	3	4	5
1	**1**	4	2	2	0
2	2	0	1	3	2
3	3	4	2	2	0
4	0	1	2	1	1
5	1	0	1	0	0

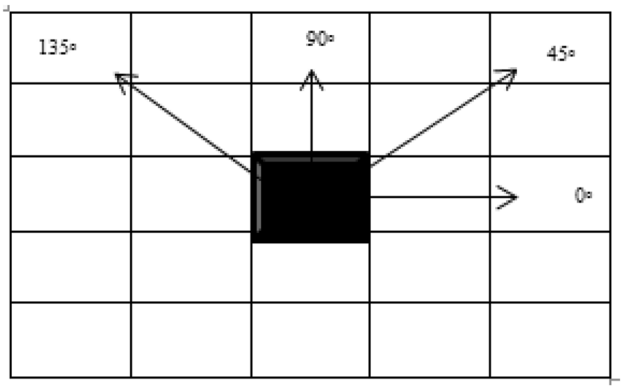

Fig. 7 Determination of Directional Co-occurance Matrices with distance d = 2 in 4 directions (angles)

The contrast feature represents the local variations in Co-Occurrence Matrix.

$$\text{Contrast} = \sum_i \sum_j P_{ij}(i-j)^2 \tag{6}$$

The correlation feature represents the combined probability of the occurrence of the specified pair of pixels.

$$\text{Correlation} = \sum_i \sum_j P_{ij} \frac{(i-\mu)(j-\mu)}{\sigma^2} \tag{7}$$

where μ is the mean of Co-Occurrence Matrix which is expressed as,

$$\mu = \sum_i \sum_j iP_{ij} \tag{8}$$

σ^2 is the variance of Co-Occurrence Matrix.

Homogeneity (Inverse Difference Moment) represents the neighborhood elements to the diagonal elements of the Co-Occurrence Matrix.

$$\text{Homogeneity} = \sum_i \sum_j \frac{P_{ij}}{1+|i-j|} \tag{9}$$

The variance feature represents the intensities of all the pixels that were in spatial relationship with each other and that are helped in building the Co-Occurrence Matrix.

$$\text{Variance} = \frac{1}{MxN} \sum_i \sum_j \left(P_{ij}-\mu\right)^2 \tag{10}$$

The Entropy feature measures the disorders of an image. When the image is non-uniform, most of the Co-Occurrence Matrix elements will have very small values. As a result, the value for the entropy becomes very large. Therefore, entropy can be said as it is inverse proportion to the Co-Occurrence Matrix energy.

$$Entropy = -\sum_i \sum_j \ln(P_{ij})P_{ij} \tag{11}$$

Algorithm of the Proposed Methodology

Input: Training Image, [I_{train}]
Output: Set of features,[F_{image}]

1) Pre-processing stage
   (i) Preprocess the input image by applying the N4 algorithm from the ANTs and BET.
   (ii) Apply the Fuzzy means clustering method to segment the Input MRI image.
   (iii) Identify the segmented image by thresholding mechanism.
2) Apply WLD to obtain the DE and GO using equations (2) and (3).
3) Perform edge enhancement to the DE and GO using equation (4).
4) Obtain the Directional Images by applying the Kirsch compass kernel method in the above two components in 8 directions as in Fig.3. Thus, obtaining 16 directional images from the two components.
5) Maximum of two-directional images are selected from the output of step 4 by computing max(d_i), where i=0,1,2,3 and max(d_i), where i=4,5,6,7. Thus, we obtain 2 directional images from each of the WLD components.
6) Obtain the directional co-occurrance matrices by applying the Co-occurance matrix method in the above 4 directional images with 2 distances (d=1 & d=2) and in 4 directions (0^o, 45^o, 90^o, 135^o). Thus, we obtain $(DE_1)_i^1$ i=1,2,3,4, $(DE_1)_j^2$ j=1,2,3,4, $(DE_2)_i^1$ i=1,2,3,4, $(DE_2)_j^2$ j=1,2,3,4, $(GO_1)_i^1$ i=1,2,3,4, $(GO_1)_j^2$ j=1,2,3,4, $(GO_2)_i^1$ i=1,2,3,4,and $(GO_2)_j^2$ i=1,2,3,4.
7) Calculate the maximum co occurance matrix based on energy.
8) Extract the statistical parameters such as contrast, correlation, mean, homogeneity, variance, entropy, sum entropy, difference entropy, prominence, and inertia by using the equations (5) to (11).
9) The set of features [F_{image}] is formed by a one-dimensional vector of features with a size of 1x88.

3.3 Classification stage

Image Classification is the technique to discriminate the data based on the specified classes. The performance of our proposed work is measured by using the two template matching methods, namely, the CS and CO and two machine learning classifiers, namely, the SVM and the ELM classifier. In addition to these classifiers, the performance is compared with the recent deep learning approach, CNN. The classification stage labels the sub-image as CMB or non-CMB using the extracted features.

4 Results and discussion

4.1 Dataset

The dataset (SWI-CMB) contains 320 SWI images [8] that are acquired from the 3.0 T Philips Medical System in which the settings are repetition time is 17 ms, volume size is $512 \times 512 \times 150$, echo time is 24 ms, the in-plane resolution is 0.45×0.45 mm, the slice thickness is 2 mm, slice spacing is 1 mm and field of view is 230×230 mm^2. From these images, images from 230 subjects of which 924 are CMBs. In this work, experiments are done in the 3D images of the axial view. The total dataset is separated into two training and testing datasets. The training dataset consists of 924 CMB images and the testing dataset consist of 225 CMB images as depicted in Table 1.

Table 1 SWI-CMB dataset overview

Dataset	Training	Testing
Subjects	230	90
CMBs	924	225

The MRI brain images that have one or more CMBs in a single image are shown in Fig. 8. These images are from the SWI-CMB database in which the CMBs are marked in green color.

4.2 Experimentation

Initially, all analyses are carried out on the training set, which contains 230 participants with 924 CMB images in SWI-CMB Dataset. The threshold mechanism is utilized to identify the correct segmented image to identify the presence of CMBs easily. To identify the segmented image, the thresholding mechanism is used. The thresholding method is needed since it reduces the false positives thereby finding the CMB mimics and reducing redundant data. The value of the threshold is chosen as 170 in our proposed methodology since the sensitivity of all the classifiers is high as tabulated in Fig. 9. By this process, only the segmented image that has CMB is selected for further processing even though practically, we will come across a few regions of mimics, which will be discriminated as non-CMB by our

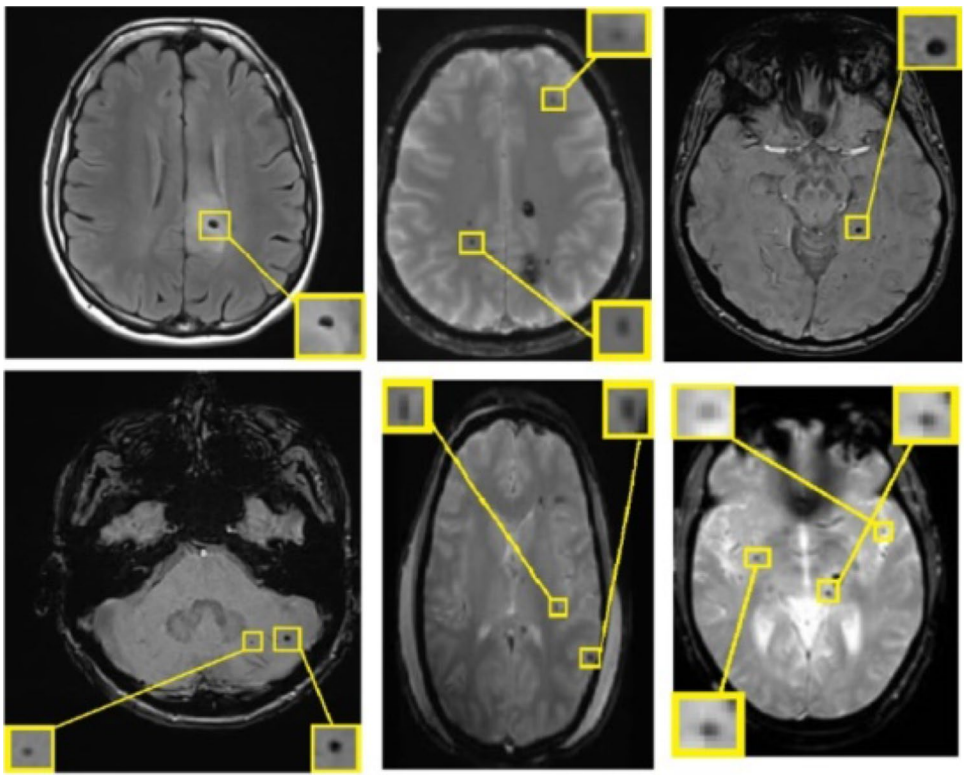

Fig. 8 Example Images from the dataset that have one or more CMBs

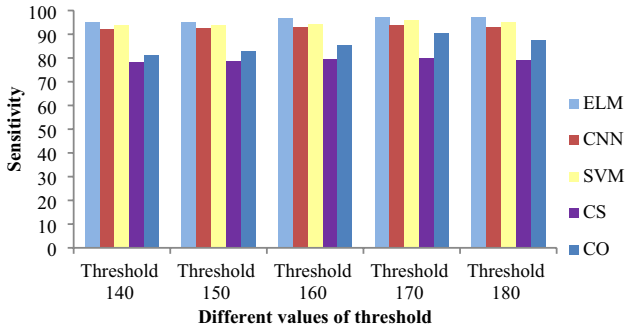

Fig. 9 Sensitivity rate of classifiers on various values of threshold

proposed method. Thus, we can get higher accuracy and sensitivity for our proposed methodology.

To improve the performance of our proposed work, after the extraction of the segmented region, we apply WLD and we obtain Differential excitation and Directional orientation components. Then, the Kirsch compass method is used to extract the directional images from which two are selected. From these two directional images, we obtain the directional magnitude co occurance matrices and directional orientation co-occurance matrices in different distances. Different directions with 0°, 45°, 90°, 135° with a distance of 1 and 2 were computed. Thus, 32 matrices are obtained from which the maximum energy matrices from both the components are chosen. The sensitivity and average false positives rate will be reasonable when the selected matrices are minimized since this reduction makes our proposed method free from computational complexity and redundancy of data. In these maximum directional co-occurance matrices and maximum orientation co-occurance matrices, the statistical parameters such as energy, entropy, homogeneity, contrast, correlation, mean, variance, sum entropy, difference entropy, shade, prominence, and inertia are computed. Thus, we obtain 88 features for a segmented region. For analysis, we consider the features obtained with distance d = 1 as feature set 1 and the features with distance d = 2 as feature set 2. Table 2 enumerates the effect of sensitivity and the average false-positive rates on the various sets of features in the proposed method.

According to the above table, when using feature set 1, we obtain a sensitivity of 85.9% and an average false positive rate of 5.3. In this case, the sensitivity is lower and the false positive rate is higher. While using feature set 2, it yielded a sensitivity of 79.83% and an average false positive rate of 8.4 percent. When both features are used together, sensitivity is enhanced to 97.11% and the average false positive rate is reduced to 3.5. We can deduce from this that the features obtained by combining both the distance values, provide better performance due to the inclusion of the maximum energy co-occurance matrices and the combination of magnitude and orientation values. Figure 10 depicts the sensitivity value as the feature counts are varied. The graph below shows that the CNN classifier performs best when the number of features is increased. CNN could not yield better results compared to ELM and SVM for our proposed feature extraction. More training data are needed for CNN to give good results. But, the features extracted by our proposed method are inadequate. Increasing the number of features by estimating more co-occurance matrix with a distance greater than 2 does

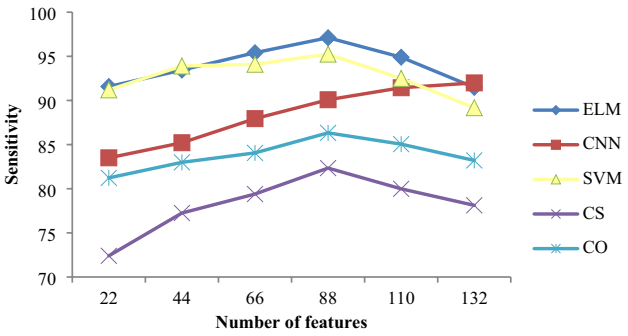

Fig. 10 Effect of feature count on sensitivity for CS, CO, SVM, ELM, and CNN classifiers

Table 2 Effect of false positives on the selected number of maximum co-occurrence matrices using ELM classifier for feature 1, feature 2, and features 1 and 2

Feature set 1 (d = 1)			Feature set 2 (d = 2)			Feature set 1 and Feature set 2		
No. of matrices	Sensitivity	Average false positives	No. of matrices	Sensitivity	Average false positives	No. of matrices	Sensitivity	Average false positives
6	82.32	6	6	78.31	7.2	12	95.67	5.1
5	83.54	5.4	5	78.02	7	10	96.68	4.7
4	85.90	5.3	4	79.83	8.4	**8**	**97.11**	**3.5**
3	84.65	5.7	3	74.56	6.2	6	97.02	3.9
2	83.05	6.34	2	72.33	6.5	4	96.48	4.5

Bold represents the maximum result obtained

Predicted Class

Actual Class	CMB	Non-CMB
CMB	**98.06%**	1.94%
Non-CMB	4.98%	**95.02%**

Predicted Class

Actual Class	CMB	Non-CMB
CMB	97.8%	2.23%
Non-CMB	6.14%	93.86%

Predicted Class

Actual Class	CMB	Non-CMB
CMB	94.58%	5.42%
Non-CMB	8.98%	91.02%

Predicted Class

Actual Class	CMB	Non-CMB
CMB	91.1%	8.9%
Non-CMB	10.57%	89.42%

Predicted Class

Actual Class	CMB	Non-CMB
CMB	90.58%	9.4%
Non-CMB	11.11%	89%

Fig. 11 Confusion Matrix for ELM, CNN, SVM, CO, and CS Classifiers

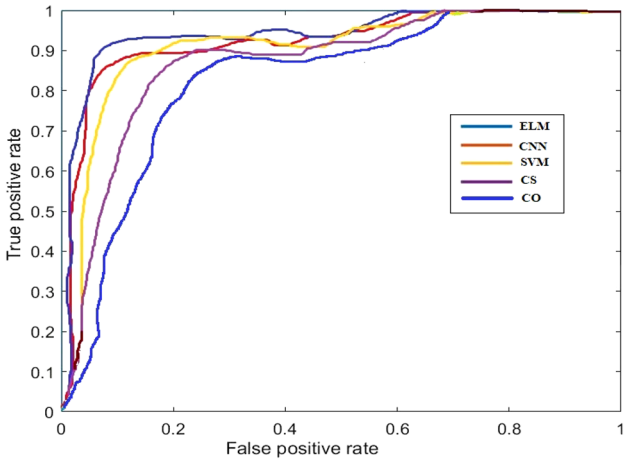

Fig. 12 ROC curve for various classifiers

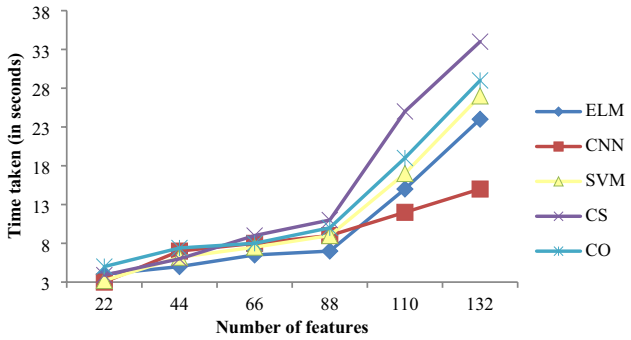

Fig. 13 The effect of the number of features on the computational time for ELM, SVM, CO, and CS classifiers

not give prominent features for classification. Hence, the distance is limited with distance 2 in the proposed work.

Figure 11 shows the confusion matrix for the ELM, CNN, SVM, CO, and CS classifiers. The performance of the proposed technique is measured using the parameters such as sensitivity, precision, accuracy, and specificity. The mathematical representations of the above parameters are given in Eqs. (12)–(15).

$$\text{Sensitivity} = \frac{True\ positive}{True\ positive + False\ negative} \tag{12}$$

$$\text{Precision} = \frac{True\ positive}{True\ positive + False\ positive} \tag{13}$$

$$\text{Accuracy} = \frac{True\ positive + True\ negative}{True\ positive + True\ negative + False\ positives + False\ Negative} \tag{14}$$

Table 3 Performance of the proposed feature extraction technique in the ten-fold Cross-Validation procedure for the test dataset

Test set	Sensitivity	Precision	Specificity	Accuracy
Fold 1	97.28	97.95	98.89	97.98
Fold 2	97.33	97.99	97.5	99.98
Fold 3	98.68	99.34	96.88	98.37
Fold 4	98.68	99.3	96.97	98.37
Fold 5	97.93	98.61	95.87	97.28
Fold 6	97.97	98.64	94.44	97.28
Fold 7	97.22	97.22	98.6	97.65
Fold 8	97.18	95.83	95.71	98.57
Fold 9	94.89	94.89	98.11	97.39
Fold 10	94.03	93.33	99.47	97.76
Average fold	97.11	97.31	97.24	98.06

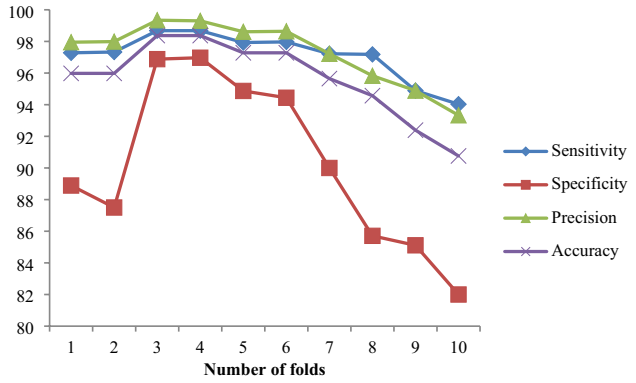

Fig. 14 Effect of the evaluation parameters in the number of folds

Table 4 Optimized hyperparameters of ELM, CNN, SVM, CS and CO classifiers

Classifiers	Optimized hyperparameters	Value
ELM	Number of hidden nodes	50
CNN	Maxepochs	10
	Initial learning rate	$1e^{-2}$
SVM (RBF kernel)	δ	2
	ω	2^6
	c	1
CS	Eigenvalue	140
CO	Eigenvalue	120

$$\text{Specificity} = \frac{True\ Negative}{True\ Negative + False\ positive} \tag{15}$$

4.3 Discussions

The ROC curves in Fig. 12 show the performance comparison of various classifiers. The ELM classifier performs well when compared with the other classifiers. The key advantages of ELM are its minimum learning capabilities, simple and automatic classification, and lack of human participation.

The evaluation is done to check the effect of the number of features count on sensitivity and computational time. In Fig. 12, the time taken for the computation of ELM, SVM, CO, CS, and CNN classifiers concerning the effect on the number of extracted feature count is plotted and evaluated. The time taken for the computation of all the five classifiers is comparable. When the number of features gets increased, the computational time also gets increased in all the classifiers except the CNN classifier. The CNN classifier shows its best performance whenever we use more data, therefore the curve is almost a straight line in Fig. 13.

The evaluation is done on the performance metrics of the feature extraction techniques. Table 3 summarizes the validation results in which the values of sensitivity, precision, specificity, and accuracy are calculated. From this validation fold, we get the average value of sensitivity as 97.11%, precision

Table 5 Performance comparison of the proposed method with the existing methods

References	Method	Performance		Time/subject
		Sensitivity	Precision	
Seghier et al. (2011)	MIDAS	50%	–	< 3 min
Barnes et al. (2011)	Statistical Thresholding Algorithm	81.7%	–	Reduced time
Bian et al. (2013)	2D Radial Symmetry Transform	86.0.5%	–	1 min
Fazlollahi et al. (2014)	Radon based features + Radom Forest Classifier	92.04%	–	-
Kuijf et al. (2012)	3D Radial Symmetry Transform	71.20%	13.20%	1.5 min
Dou et al. (2015)	3D hierarchical features and Independent Subspace Analysis (ISA) network	89.44%	–	40 s
Van Den Heuvel et al. (2015)	Computer Aided Detection (CAD)	90%	–	–
Dou et al. (2016)	3D Convolutional Neural Network (CNN)	93.2%	44.31%	64 s
Wang et al. (2017)	Convolution Neural Network With Rank Based Average Pooling	96.94%	–	–
Liu et al. (2019)	3D-ResNet	95.8%	70.90%	9 s
Chen et al. (2019)	3D-ResNet	94.69%	71.98%	–
Hong et al. (2019)	2D-ResNet-50	95.71%	–	–
Al-masni et al. (2020)	YOLO & 3D CNN	93.62%	36.26%	33 s
Liu et al. (2020)	Fourier descriptor with dual domain distribution modeling	85.2%	–	–
Koschmieder et al. (2022)	CNN & U-Net	90%	–	–
Proposed work	Edge Emphasized Weber Maximum Directional Co-Occurance Matrix (EEWMDCM)	97.11%	97.31%	7 s

value as 97.31%, specificity value as 97.24%, and accuracy value as 98.06%.

Figure 14 shows the effect of sensitivity, specificity, precision, and accuracy depending on the varying folds from 1 to 10. Here, the value of accuracy and specificity is almost equipollent, other parameters are comparable.

The optimized hyperparameters of the ELM, CNN, SVM, CS and CO classifiers are listed in Table 4. The number of hidden nodes in ELM is 50. The CNN has the maximum epoch of 10. In SVM, δ represents the kernel values and c represents the penalty parameter. The hyperparameters of CS and CO are in terms of eigenvalues which are 140 and 120 respectively.

Table 5 compares our current state of work to the established methodologies. In recent years, many analyses and initiatives have been organized for computer-aided detection of CMBs. The major critical problem is distinguishing actual CMBs from false CMBs such as calcifications to make an accurate diagnosis and provide the appropriate treatment. In the current context, the development of Susceptibility Weighted Imaging (SWI) is a critical source for the enhanced visibility of cerebral veins. The reason for this is that the vulnerability of local tissue and microbleeds is only highly sensitive in SWI images.

The FRST is one of the strategies that use local radial symmetry to identify spherical regions in brain imaging. It should be highlighted that the suggested method outperforms the most generally used FRST method for detecting CMBs, achieving high sensitivity and a low number of false positives per person. 3D-FRST is used to test the ability to discover CMB prospective candidates in comparison to the suggested work. The 3D-FRST worked with more sensitivity, but at the same time generated more umber of FPs per subject. The proposed method generated an average false positive rate of 3.5 with a sensitivity of 97.11%.

The 3D-FRST method which is used in Kuijf et al. (2011) has many limitations. One such limitation is that even after intensifying the CMB samples, robust numbers of training samples are generated. This generation of huge samples diminishes the performance. The result of 3D-CNN also shows that it does not affect the FP, but it reduces sensitivity. High performance in terms of sensitivity and precision can be noticed and achieved in Chen et al. (2019), Liu et al. (2019), Wang et al. (2019), and Hong et al. (2019) which are due to the large number of CMB images used for the analysis purposes when compared with the existing studies. The number of input images used by Liu et al. (2019) is 1641 CMB images from 220 subjects, Chen et al. (2019) used 73 subjects from which the number of images extracted is 2835, Wang et al. (2019) experimented with 68,847 CMB images from 20 patients and the number of images selected for experimentation in Hong et al. (2019) is 4287 CMBs from 10 subjects. Wang et al. (2017) proposed a five-layer CNN which produced a sensitivity of 96.94%, specificity of 97.18%, and an accuracy of 97.18%. Koschmieder et al. (2022) experimented the presence of CMB in the dataset that contained 45 images and obtained a sensitivity of 90%. In all the above existing works, deep learning approaches are used. Even though it has an attractive behavior in medical applications, several drawbacks arise. The drawbacks are since the MRI Images are 3D it has multiple contrast images, the imaging parameters varies from scan to scan, need for a huge number of images. The proposed work is an effective method when compared to the other methods with lower computation time. It only requires 7 s to process and generate its associated potential candidates.

5 Conclusion

The early detection of CMBs bumper the human from getting into related diseases. An efficient method was presented for detecting CMBs using WLD and Co-occurance Matrices in this study. The Kirsch compass approach improves the performance of the proposed work, and the application of SWI Images improves the accuracy rate to detect the CMBs. Because of the ELM classifier, the computational cost and complexity are both minimal. The proposed approach performs better when there is more than one CMB in an image, and it also performs better when employed on smaller datasets. The experimental results suggest that the proposed method outperforms existing methods in detecting actual CMBs with a sensitivity of 97.11%, a precision of 97.31%, specificity of 97.24%, and an accuracy of 98.06%. The proposed method can also be applied to other studies in the different detecting sectors.

Our concept has a few drawbacks, which we intend to address in the future. The first limitation is that the proposed method classifies only two sets of classes. The second limitation is that whenever the dataset for training is large, it takes more time than expected to reach the goal. To overcome these limitations in the future, more classes can be included such as gray matter, background, white matter. Larger datasets can be collected from the reputed hospitals, in which the data will be more in number. Analyzing more images increases the robustness and reliability of the proposed work. Also, the proposed work can be used with modern classifier techniques to check its performance.

Funding Not applicable. We did not get any funds for this research work.

Declarations

Conflict of interest The authors declare that they have no conflict of interest.

Ethical approval This research work does not contain any studies with animals performed by any of the authors.

References

Abdalzaher MS et al (2021a) Comparative performance assessments of machine-learning methods for artificial seismic sources discrimination. IEEE Access 9:65524–65535

Abdalzaher MS, Soliman MS, El-Hady SM, Benslimane A, Elwekeil M (2021b) A deep learning model for earthquake parameters observation in IoT system-based earthquake early warning. IEEE Internet Things J. https://doi.org/10.1109/JIOT.2021.3114420

Abro WA, Qi G, Ali Z, Feng Y, Aamir M (2020) Multi-turn intent determination and slot filling with neural networks and regular expressions. Knowl-Based Syst 208:106428. https://doi.org/10.1016/j.knosys.2020.106428

Al-masni MA, Kim W-R, Kim EY, Noh Y, Kim D-H (2020) Automated detection of cerebral microbleeds in MR images: a two-stage deep learning approach. NeuroImage Clin 28:2020. https://doi.org/10.1016/j.nicl.2020.102464

Barnes SRS, Haacke EM, Ayaz M, Boikov AS, Kirsch W, Kido D (2011) Semiautomated detection of cerebral microbleeds in magnetic resonance images. Magn Reson Imaging 29(6):844–852. https://doi.org/10.1016/j.mri.2011.02.028

Bian W, Hess CP, Chang SM, Nelson SJ, Lupo JM (2013) Computer-aided detection of radiation-induced cerebral microbleeds on susceptibility-weighted MR images. NeuroImage Clin 2:282–290. https://doi.org/10.1016/j.nicl.2013.01.012

Charidimou A, Krishnan A, Werring DJ, Jager HR (2013) Cerebral microbleeds: a guide to detection and clinical relevance in different disease settings. Neuro-Radiology 74:655–674. https://doi.org/10.1007/s00234-013-1175-4

Chen J, Shan S, He C, Zhao G, Chen MPJ, Shan S, Chu He X, Chen WG (2010) WLD: a robust local image descriptor. IEEE Trans Pattern Anal Mach Intell 32:1705–1720

Chen Y, Villanueva-Meyer JE, Morrison MA, Lupo JM (2019) Toward automatic detection of radiation-induced cerebral microbleeds using a 3D deep residual network. J Dig Imaging 32:898–898. https://doi.org/10.1007/s10278-018-0146-z

Conners RW, Trivedi MM, Harlow CA (1984) Segmentation of a high-resolution urban scene using texture operators. Comput vis Graph Image Process 25:273–310

Dou Q, Chen H, Yu LQ, Zhao L, Qin J, Wang DF, Mok VCT, Shi L, Heng PA (2016) Automatic detection of cerebral microbleeds from MR images via 3D convolutional neural networks. IEEE Trans Med Imaging 2016:1182–1195. https://doi.org/10.1109/TMI.2016.2528129

Dou Q, Chen H, Yu L, Shi L, Wang D, Mok VC, Heng PA (2015) Automatic cerebral microbleeds detection from MR images via independent subspace analysis based hierarchical features. In: 37th annual international conference of the IEEE engineering in medicine and biology society (EMBC), pp 7933-6

Fazlollahi A, Meriaudeau F, Villemagne VL, Rowe C, Yates P, Salvado O, Bourgeat PT (2014) Efficient machine learning framework for computer-aided detection of cerebral microbleeds using the radon transform. In: Proceedings of the IEEE-ISBI conference

Greenberg SM, Vernooij MW, Cordonnier C, Viswanathan A, Al-Shahi Salman R, Warach S et al (2009) Cerebral microbleeds: a guide to detection and interpretation. Lancet Neurol 8(2):165–174

Haralick RM, Shanmugam K, Dinstein I (1973) Textural features for image classification. IEEE Trans Syst Man Cybern 3:610–621

Van den Heuvel T, Ghafoorian M, van der Eerden A, Goraj B, Andriessen T, ter Haar Romeny B, Platel B (2015) Computer aided detection of brain micro-bleeds in traumatic brain injury. In: SPIE medical imaging international society for optics and photonics, pp 94142F–94142F. https://doi.org/10.1117/12.2075353

Hong J, Cheng H, Zhang YD, Liu J (2019) Detecting cerebral microbleeds with transfer learning. Mach vis Appl 2019:1123–1133

Kirsch R (1971) Computer determination of the constituent structure of biological images. Comput Biomed Res 4:315–328

Koschmieder K, Paul MM, den Heuvel TLA, der Eerden AW, Ginneken B, Manniesing R (2022) Automated detection of cerebral microbleeds via segmentation in susceptibility-weighted images of patients with traumatic brain injury. NeuroImage Clin 35:103027. https://doi.org/10.1016/j.nicl.2022.103027

Kuijf HJ, de Bresser J, Biessels GJ, Viergever MA, Vincken KL (2011) Detecting cerebral microbleeds in 7.0 T MR images using the radial symmetry transform. In: 2011 IEEE international symposium on biomedical imaging: from nano to macro, pp 758–761

Kuijf HJ, de Bresser J, Geerlings MI, Conijn M, Viergever MA, Biessels GJ, Vincken KL (2012) Efficient detection of cerebral microbleeds on 7.0 T MR images using the radial symmetry transform. Neuroimage 59:2266–2273. https://doi.org/10.1016/j.neuroimage.2011.09.061

Liu SF, Utriainen D, Chai C, Chen YS, Wang L, Sethi SK, Xia S, Haacke EM (2019) Cerebral microbleed detection using Susceptibility Weighted Imaging and deep learning. Neuroimage 198:271–282

Liu H, Rashid T, Habes M (2020) Cerebral microbleed detection via fourier descriptor with dual domain distribution modeling. In: 2020 IEEE 17th international symposium on biomedical imaging workshops, pp 1–4. https://doi.org/10.1109/ISBIWorkshops50223.2020.9153365

Marcel P, Elizabeth B, Guido G (2009) Simulation of brain tumors in MR images for evaluation of segmentation efficacy, Medical Image Analysis, Elsevier

Martinez-Ramirez S, Greenberg SM, Viswanathan A (2014) Cerebral microbleeds: overview and implications in cognitive impairment. Alzheim Res Therapy 6:33. https://doi.org/10.1186/alzrt263

Mohammed K, Habib A, Abdellah A (2018) Performance evaluation of feature extraction techniques in MR-Brain image classification system. Procedia Comput Sci 127:218–225. https://doi.org/10.1016/j.procs.2018.01.117

Moustafa SSR, Abdalzaher MS, Yassien MH, Wang T, Elwekeil M, Hafiez HEA (2021) Development of an optimized regression model to predict blast-driven ground vibrations. IEEE Access 9:31826–31841. https://doi.org/10.1109/ACCESS.2021.3059018

Sangiem S, Dittakan K, Temkiavises K, Yaisoongnern S (2019) Cerebral mirobleed detection by extracting area and number from susceptibility weighted imagery using convolutional neural network. J Phys Conf Ser 1229:012038. https://doi.org/10.1088/1742-6596/1229/1/012038

Seghier ML, Kolanko MA, Leff AP, Jäger HR, Gregoire SM, Werring DJ (2011) Microbleed detection using automated segmentation (MIDAS): a new method applicable to standard clinical MR images. PLoS ONE 6:e17547

Smith SM (2002) Fast robust automated brain extraction. Hum Brain Mapp 17(3):143–155

Stanley BF, Wilfred-Franklin S (2022) Automated cerebral microbleed detection using selective 3D gradient co-occurance matrix and convolutional neural network. Biomed Signal Process Control 75:103560. https://doi.org/10.1016/j.bspc.2022.103560

Tustison NJ, Avants BB, Cook PA, Zheng Y, Egan A, Yushkevich PA et al (2010) N4ITK: improved N3 bias correction. IEEE Trans Med Imaging 29(6):1310–1320

Ullah I, Jian M, Khan S, Lian L, Ali Z, Qureshi I, Jie G, Yin Y (2021) Global context-aware multi-scale features aggregative network for salient object detection. Neurocomputing 455:139–153. https://doi.org/10.1016/j.neucom.2021.05.001

Wang S, Jiang Y, Xiaoxia H, Cheng H, Du S (2017) Cerebral micro-bleed detection based on the convolution neural network with rank based

average pooling. IEEE Access 2017:1–1. https://doi.org/10.1109/ACCESS.2017.2736558

Wang SH, Tang CS, Sun JD, Zhang YD (2019) Cerebral micro-bleeding detection based on densely connected neural network. Front Neurosci 2019:13

Yates PA, Villemagne VL, Ellis KA, Desmond PM, Masters CL, Rowe CC (2014) Cerebral microbleeds: a review of clinical, genetic, and neuroimaging associations. Front Neurol 4:205